Article

DLEMMA-MS-Imaging for Identification of Spatially Localized Metabolites and Metabolic Network Map Reconstruction

liron Feldberg, Yonghui Dong, Uwe Heinig, Ilana Rogachev, and Asaph Aharoni

Anal. Chem., **Just Accepted Manuscript** • DOI: 10.1021/acs.analchem.8b01644 • Publication Date (Web): 31 Jul 2018

DLEMMA-MS-Imaging for Identification of Spatially Localized Metabolites and Metabolic Network Map Reconstruction

Liron Feldberg[1,2,#,*], Yonghui Dong[1#], Uwe Heinig[1], Ilana Rogachev[1] and Asaph Aharoni[1*]

[1]Department of Plant Sciences, Weizmann Institute of Science, Rehovot, Israel

[2]Department of Analytical chemistry, Israel Institute for Biological Research, Ness Ziona, Israel

[*]Corresponding author. Tel.: +972 544 784259;

[#]These authors contributed equally to this work

E-mail: liron.feldberg@gmail.com; asaph.aharoni@weizmann.ac.il

Competing interests

The authors declare no competing financial interests.

ABSTRACT

Regardless of major advances in mass spectrometry imaging (MSI), there are three intrinsic limitations associated with MSI including intricate molecular identification, low molecular coverage and incapability to obtain 'true' spatial distribution due to isobaric and particularly isomeric ions interference. We developed a novel approach that integrates *in vivo* dual isotope labeling of precursor metabolites with MSI (DLEMMA-MS-Imaging) for identification of spatially localized metabolite and metabolic network map reconstruction. In a proof-of-concept study, we identified 59 and 6 novel metabolites in lemna and tomato fruit, respectively. Significantly, 20-30% of the identified metabolites were found to contain at least one structural isomer that displays a different distribution pattern. The notable feature of this approach is the ability to differentiate localization of structural isomers, hence providing the 'true' distribution of molecules of interest.

INTRODUCTION

Over the last decade, mass spectrometry imaging (MSI) techniques have advanced tremendously in sensitivity and spatial resolution. They have evolved as indispensable analytical tools for label-free analysis of various molecules in their native histological context[1]. Matrix-assisted laser desorption/ionization (MALDI), in particular, is one of the most wide-spread MSI approaches, leading the way in the development of biological and clinical applications for MSI assays[2].

Despite the impressive progress and applications, there are three inherent limitations associated with MSI: (i) molecular annotation is challenging. MSI experiments directly analyze molecules on a tissue surface without any extraction or chromatographic separation

step; thus the molecules are identified only according to the accurate *m/z* and MS/MS when applicable[1,3]. Although elemental composition can be determined by measuring the isotopic fine structure with ultra-high-resolution MS (mass resolution > 500,000), it does not provide unambiguous identification of isomeric compounds. MS/MS effectively narrows down the number of candidates, yet, only ions with sufficient intensities can be selected for meaningful MS/MS fragmentation. The challenge associated with MS/MS is also exacerbated when overlapping peaks are present in discrete sample regions[4,5]. (ii) Molecular coverage is typically low[6]. Owing to the high molecular complexity of the sample tissue, MSI is prone to ion suppression effects which result in a reduced capability to detect low-abundant molecular species[7,8]. Molecular coverage also declines with increasing in spatial resolution as reducing sampling area to improve spatial resolution reduces the amount of ions available for detection[9,10]. (iii) The observed MS image for single *m/z* value is at high risk of containing overlapped MS images, and as a consequence misrepresenting the true localization of the molecule of interest. For instance, MSI can hardly differentiate distribution of structural isomers which possess the same *m/z* values. In a more common case, very close *m/z* peaks (i.e. isobaric ions) may be detected as a single peak by low mass resolution MSI and therefore producing a false spatial distribution. Various strategies have been applied to alleviate some of those limitations. For instance, MS/MS imaging was employed to confirm molecular identity[6,11,12], multiplexing approach was developed to improve the molecular coverage[13], in-tissue chemical derivatization was performed to distinguish isobaric species[14], deuterium labeled-matrix was used to eliminate the matrix interferences[15], and ion mobility spectrometry (IMS) was combined with mass spectrometry to separate isobaric species[16,17]. However, the

interference of structural isomers on mapping the distribution of target metabolites in MSI has not been tackled extensively to date.

To address these key issues and advance the use of MSI technology, we have established a stable isotope assisted MSI approach that could markedly minimize the three major limitations noted above. Our lab previously developed a stable isotope-based metabolomics tool, termed DLEMMA (Dual Labeling of Metabolites for Metabolome Analysis), for high-confidence metabolite identification[18]. This approach allows the detection of downstream labeled metabolites by feeding with two forms of differentially labeled precursors using liquid chromatography coupled to high resolution mass spectrometry. Compared to the 'classical' single form labeled precursor based approach, DLEMMA largely narrows down the number of structural isomer candidates for a given elemental composition since it accurately pinpoints the position of loss or retention of labeled atoms. It is worth noting that a single labeled precursor based approach has been applied in MSI for qualitative, quantitative or kinetic analysis[19-22]. We thus anticipated that combining DLEMMA with MSI will increase the benefit derived from stable isotope labeling and circumvent the above-mentioned limitations in MSI.

Experimental Section

Chemicals and Reagents

Tyrosine (> 98%) and phenylalanine (> 98%) were purchased from Sigma-Aldrich (Israel). Tyrosine D4 (D > 98%), tyrosine $^{13}C_9{}^{15}N_1$ (13C > 98%, 15N > 98%), phenylalanine D5 (D > 98%), phenylalanine $^{13}C_9{}^{15}N_1$ (13C > 99%, 15N > 99%) were synthesized by Cambridge Isotope Laboratories (Andover, MA).

Plant material and feeding experiments

Lemna fronds (*Spirodela polyrhiza*) were propagated at 26 °C, 30-50 µmol $m^{-2}s^{-1}$ cool white fluorescent light and 5% CO_2 in 250-ml Erlenmeyer flasks containing 80 ml half-strength Hutner's solution (SP medium)[23]. Plants were pre-cultivated for 4 weeks and the medium was replaced with fresh medium every week. Two-frond colonies, obtained from this pre-cultivation, were used for tyrosine feeding. The feeding experiments for DLEMMA consisted of 5 groups with each group containing 6 two-frond colonies: Group A (SP medium), Group B (0.5 mg ml^{-1} Unlabeled tyrosine), Group C (0.5 mg ml^{-1} tyrosine D_4, Label I), Group D (0.5 mg ml^{-1} tyrosine $^{13}C_9{}^{15}N_1$, Label II) and Group E (0.5 mg ml^{-1} Label I + Label II) (Fig. 1). The feeding experiments for MALDI imaging included two groups: Group A (SP medium) and Group E (0.5 mg ml^{-1} Unlabeled tyrosine + Label I + Label II). The feeding experiments were performed under the same lemna frond propagation conditions for 24 hours. Tomato plants (*S. lycopersicum*, cv. Microtom) were grown in a climate-controlled greenhouse at 24/18°C (day/night) at natural day length conditions[24]. Fruit at the orange stage, which were on average 41 d after anthesis, were collected for feeding. The tomato fruit feeding was performed as described above for lemna and DLEMMA experiment includes 5 groups: Group A (water), Group B (5 mg ml^{-1} Unlabeled phenylalanine), Group C (5 mg ml^{-1} phenylalanine D_5, Label I), Group D (5 mg ml^{-1} phenylalanine $^{13}C_9{}^{15}N_1$, Label II) and Group E (5 mg ml^{-1} Label I + Label II). MALDI imaging consists of 2 groups: Group A (water) and Group E (5 mg ml^{-1} Unlabeled phenylalanine + Label I + Label II). The fruit were excised with a new razor blade leaving approximately 1.5 cm of the pedicel attached. They were first incubated in a controlled temperature at 25 °C with the cut surface of the pedicel submerged in EDTA solution (20 mM) for 1h to improve the feeding efficiency by inhibiting callus formation in the cut surface of the phloem[25,26]. The fruit were then immerged into each

feeding solution for 3 d. During this time, 0.3 ml feeding solution was added every day to each corresponding feeding group to ensure that the cut surface of the pedicel was continuously submerged.

UPLC–ESI-QTOF-MS/MS

Chromatographic experiments were performed on a UPLC-QTOF system (HDMS Synapt, Waters). UPLC separation was performed on a Waters ACQUITY™ UPLC™ BEH C18 column (100 × 2.1 mm, 1.7 μm) with the column temperature set at 35 °C. The mobile phase consisted of 0.1% formic acid in acetonitrile: water (5:95, v/v, phase A) and 0.1% formic acid (v/v) in acetonitrile (phase B). The LC method was as follows: the linear gradient was from 100 to 72% phase A over 22 min, from 72 to 0% phase A over 14 min, then held at 100% phase B for further 2 min; and then returned to the initial conditions (100% phase A) in 0.5 min and conditioning at 100% phase A for 1.5 min. A divert valve (Rheodyne) excluded the first 1 min and last 2 min of gradient from the injection. Data acquisition was performed in the MS^E mode with energy ramp that records an accurate mass precursor and fragment ion information from every detectable component in a sample. The MS^E mode rapidly alternates between two functions: the first acquiring low-energy accurate mass precursor ion spectra and the second acquiring elevated-energy accurate mass fragment ion spectra. The collision energy was set to 4 eV for the low-energy function and to 10–30 eV ramp for the high-energy function in the positive ion mode (15-35 eV in the negative ion mode). Scan time for each function was set to 0.25 s. The MS^E mode with energy ramp was used to add as much of the specific fragmentation patterns of each metabolite as possible in one continuous run. LC-MS/MS experiments were run using the following settings: capillary spray at 1.0 kV; cone voltage at 27 eV; collision energies were 10 - 25 eV for the positive mode and 15-40 for the

negative mode. Argon was used as the collision gas for collision-induced dissociation (CID). In addition, a mixture of 15 standard metabolites, injected after each 10 samples, was used for quality control.

LC-MS Data processing

The raw instrument data were first converted to NetCDF format using MassLynx Databridge (http://www.waters.com). The NetCDF files containing data from the first and second MS channels were then converted into data matrices using the R (http://www.r-project.org) packages XCMS[27]. The pre-processing stage generated a single peak matrix for each injection, containing the m/z, RT and peak intensity profiles. The labeled analytes were extracted with home-written R package (Tutorial S1).

MALDI imaging

Lemna plants were washed gently with distilled water, dried using a stream of nitrogen gas, attached onto glass slides using double-sided tape, and subsequently desiccated under moderate vacuum for 1h to minimize metabolite turnover[7]. Fresh tomato fruit were embedded with M1 embedding matrix (Thermo Scientific, Waltham, MA) in Peel-A-Way disposable embedding molds (Peel-A-Way Scientific, South El Monte, California), and flash-frozen in liquid nitrogen. The embedded tissues were transferred to a cryostat (Leica CM3050) and allowed to thermally equilibrate at -18 °C for 1hour. The frozen tissues were cut into 35-µm-thick sections which were thaw mounted onto Superfrost Plus slides (Fisher Scientific, Pittsburg, PA) and vacuum dried in a desiccator. An ImagePrep spray station (Bruker Daltonics, Germany) was used to coat the slide with the DHB matrix ($30\,g\,L^{-1}$ in water/methanol, v/v, 50/50 containing 0.2% trifluoroacetic acid). The system settings were as follows: 50 spray cycles, 50% sprayer power, 20% modulation, 2 s spray, 2 s incubation, and

70 s dry time. MALDI imaging measurements were performed using a 7T Solarix FT-ICR (Fourier transform ion cyclotron resonance) mass spectrometer (Bruker Daltonics, Bremen, Germany). MSI datasets were collected in the positive mode using lock mass calibration (DHB matrix peak: m/z 409.055408) in the range 150–3000 m/z, with a spatial resolution of 65 µm. Each mass spectrum was obtained from a single scan of 100 laser shots at a frequency of 1 kHz and a laser power of 18%. The acquired spectra were processed using the FlexImaging software v. 4.0 (Bruker Daltonics, Germany). Data sets were normalized to root mean square (RMS) intensity and MALDI images were plotted at the theoretical *m/z* ± 0.001%, with pixel interpolation on.

RESULTS AND DISCUSSION

The concept of DLEMMA-MS-Imaging was demonstrated in two plant species, namely, lemna (*Spirodela polyrhiza*) and tomato (*Solanum lycopersicum*). Intact lemna plants were fed with tyrosine (unlabeled Tyr, Tyr$^{2}H_4$ and Tyr$^{13}C_9{}^{15}N$) and tomato fruit (detached) with phenylalanine (unlabeled Phe, Phe$^{2}H_5$ and Phe$^{13}C_9{}^{15}N$). Tyrosine and phenylalanine were chosen as feeding precursors since they are major hubs in the plant metabolic network through which enormous carbons flow towards primary and secondary metabolism[28]. In brief, a complete DLEMMA-MALDI-Imaging setup integrates a five-component LC-MS with a two-component MALDI imaging experiments. The five-component LC-MS experiment includes: (i) control: samples without feeding, (ii) samples fed with unlabeled precursor, (iii) samples fed with labeled I precursor, (iv) samples fed with labeled II precursor, and (v) samples fed with a mixture of two labeled precursors. The two-component MALDI Imaging experiment includes: (i) control: samples without feeding, and (ii) samples fed with a mixture of unlabeled and two labeled precursors (Fig. 1). Samples were analyzed in both positive and negative ion modes, and

metabolites were identified considering their retention times, accurate *m/z* values, MS/MS spectra, dual-labeling patterns and distribution patterns. The precision obtained for biological replicates (3 replicates for each metabolite) is in the range of 10%-50% with an average relative standard deviation (RSD) of 30%. The spatial distribution pattern of each metabolite is found consistent among the three biological replicates for each experiment. Details regarding the experimental workflow, data analysis (including an R package for isotope filtering developed in-house) and a step-by-step tutorial are provided in Tutorial S1.

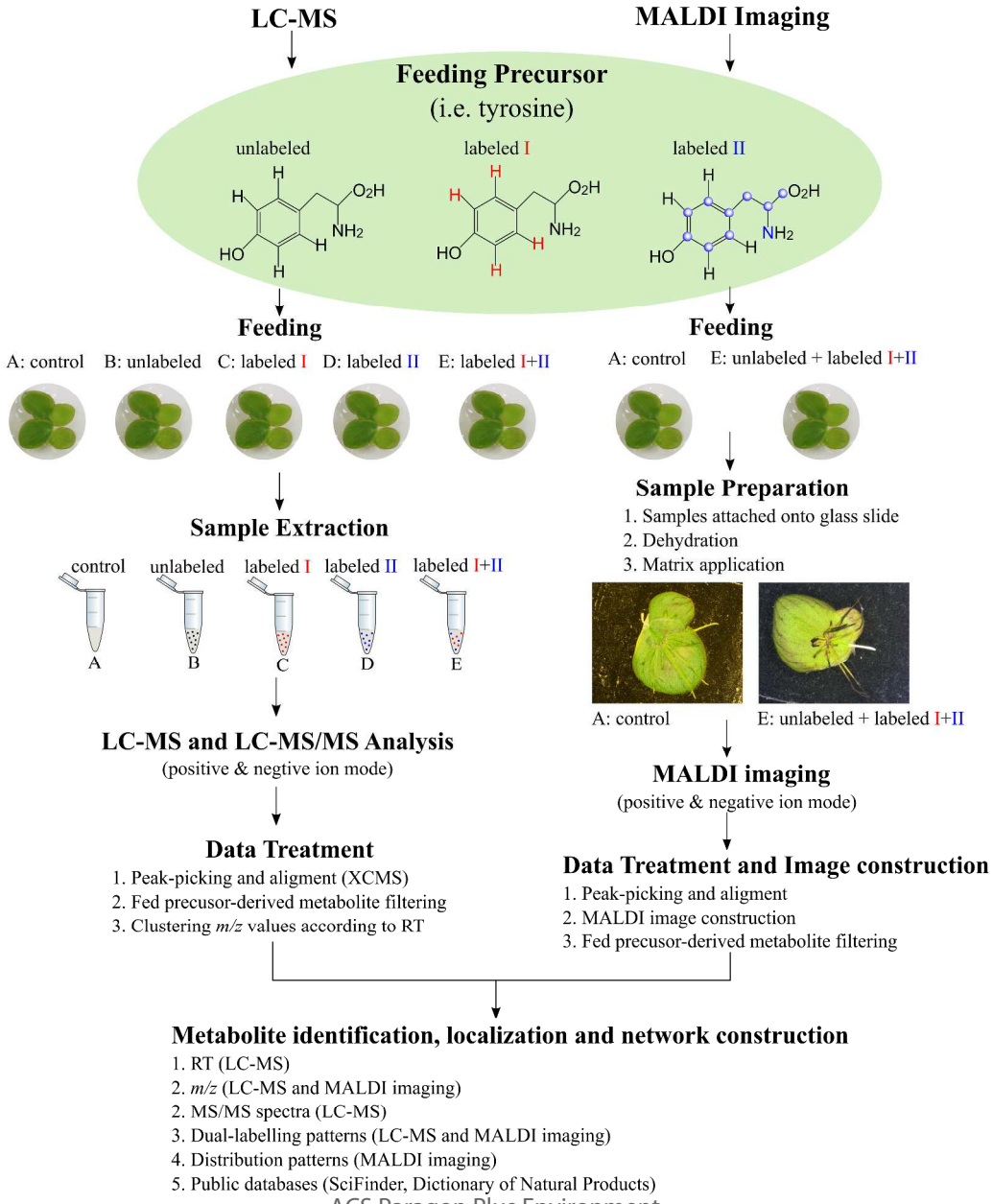

Figure 1. Schematic representation of the DLEMMA-MALDI-Imaging methodology. LC-MS and MALDI imaging experiments within the platform share several common steps: feeding, sample preparation, sample analysis and data processing. The workflow begins by feeding samples with 3 forms of precursors (one unlabeled and two precursors labeled in a different way). Fed samples are subjected to LC-MS and MALDI imaging in both positive and negative ion modes. The LC-MS raw data is preprocessed and next a home-written R package is used to detect and filter the fed precursor-derived metabolites. MALDI imaging results are processed and visualized using MS imaging software such as FlexImaging. The fed precursor-derived metabolites are identified taking into account retention time, *m/z*, MS/MS spectra and dual-labeling patterns from LC-MS, and *m/z*, dual-labeling patterns and distribution patterns from MALDI imaging.

One of the notable features of DLEMMA-MALDI-Imaging is high-confidence metabolite identification. The use of two differently labeled precursors provides detailed structural information which could be used to facilitate metabolite identification. The workflow of metabolite identification through DLEMMA-MALDI-Imaging is presented in Figure 2. First, an automated labeled analyte search was performed in the LC-MS and MALDI imaging peak lists using a home-written R package, and only the isotopically labeled and their corresponding unlabeled analytes were kept. The peak lists were typically reduced from 20,000 to about 100 after isotope-pattern-filtering (step 1). The filtered peak list was then used for metabolite identification. For instance, LC-MS analysis of lemna fed with unlabeled and two differently labeled tyrosines (unlabeled Tyr, Tyr$^{2}H_4$ and Tyr$^{13}C_9{}^{15}N$) showed that the metabolite *m/z* 267.1345 displayed the labeling patterns of *m/z*+$^{2}H_4$ (4 labeled atoms in experiment group C) and m/z +$^{13}C_8{}^{15}N_1$ (9 labeled atoms in experiment group D). The elemental composition of this

metabolite was determined based on its accurate *m/z* and natural isotope pattern (step 2). However, the database search (i.e., using SciFinder) revealed that there were more than 15,000 candidates for its elemental composition ($C_{13}H_{18}N_2O_4$; step 3). As this metabolite was labeled with 4 deuterium it must contain an aromatic ring as tyrosine. This structure restricted search using the structural information provided by experiment group C reduced the number of candidates from 15,000 to 313 (step 4). Similarly, the number of candidates was reduced to 403 considering the structural information obtained from group D (step 5). When the structural information from both experimental group C and D were taken into account, the number of candidates was reduced significantly to 48 candidates, and among them 4 were reported in biological samples (step 6). Based on the MS/MS information this metabolite was finally identified as glutamine (step 7). To improve the throughput of metabolite identification, the isotope-pattern-filtered peak lists could be matched against a home mass spectral library or a list of target compounds. The isotope labeling patterns and MS/MS fragments are only used to confirm the identification. Only the remaining unknown analytes should be searched in SciFinder or other databases following the steps described above. As ionization mechanisms are different between ESI and MALDI, not all metabolites that are ionized by ESI using LC-MS will be necessarily ionized by MALDI, and vice versa. As such, mass matching between LC-MS and MALDI imaging peak lists is usually challenging. A common way is to match the peak list from MALDI imaging with that from LC-MS using accurate *m/z* values[29]. However this approach can lead to false positives due to the presence of background peaks. Since mass matching was performed using only isotopically filtered peak lists obtained from DLEMMA-MALDI-Imaging, the disturbance of background peaks was reduced; moreover all the unlabeled and labeled peaks

were considered for mass matched, which largely improves the confidence in matching of MALDI imaging peak list to LC-MS peak list used for identification.

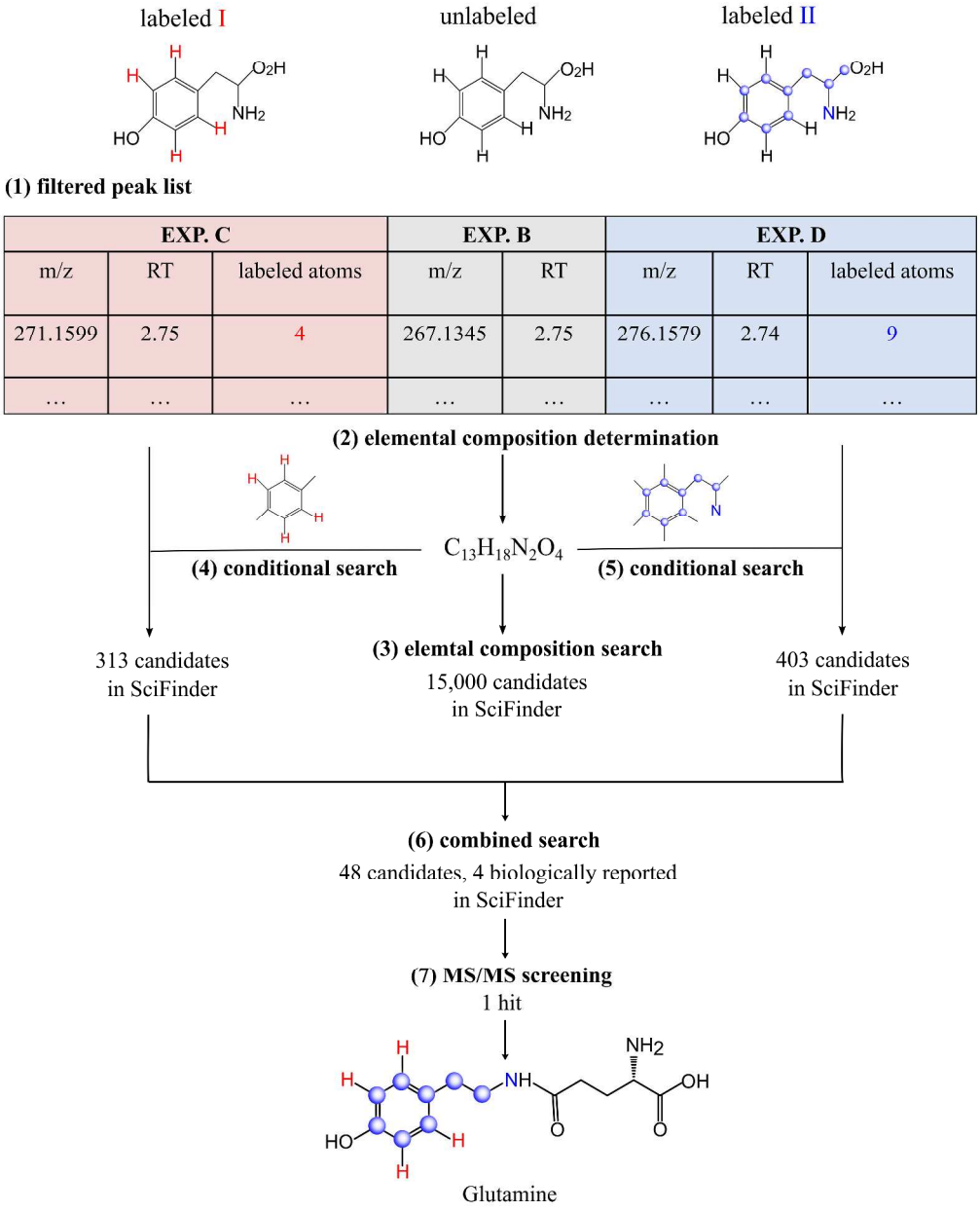

Figure 2. A representative workflow for metabolite identification in DLEMMA-MALDI-Imaging. An automated labeled analyte search was first performed on LC-MS and MALDI imaging peak lists and only the filtered peak lists were used for metabolite identification.

Elemental composition is determined for each analyte in the unlabeled precursor feeding group (experimental group B) based on the accurate *m/z* and natural isotope pattern. The structural information from the labeling groups (experimental group C and D) is then used to narrow down the candidates found in a database (i.e., SciFinder). The MS/MS pattern is finally used to infer the structure and screen the candidates.

Following the approach presented above, sixty tyrosine-derived metabolites were identified in lemna for the first time (Table S1), in which 59 have never been reported in this species. It is worth noting that half of them were detected due to increased concentration as a result of tyrosine feeding. Nevertheless, they are most likely not a result of stress induction due to tyrosine feeding as they were all without exception detected in non-feeding group after concentrating the plant extract (albeit in much smaller amounts as compared to the tyrosine fed samples). This highlights the advantage of precursor feeding for increasing molecular coverage. Once the tyrosine-derived metabolites were identified we were able to construct a detailed metabolic network map including about half of the identified lemna metabolites based on their labeling patterns and known biochemical reactions (Fig. 3). This predicted metabolic network begins with tyrosine that can be metabolized in four different ways, transamination, dimerization (of decarboxylated and deaminated tyrosine-derived metabolites), hydroxylation of the aromatic ring and decarboxylation followed by deamination. The resulting tyrosine-derived metabolites are further metabolized through more than one route to form branched pathways following various metabolic reactions. The labeling efficiency decreases with increase in size of the metabolic pathway. A genetic knockout strategy can be subsequently employed to validate the pathway and determine candidate enzymes and genes. Remarkably, all glycosylated metabolites

were found to be localized in the roots. With the same approach, 28 phenylalanine-derived metabolites were identified in tomato fruit, in which 6 have never been reported in this tissue (Table S2).

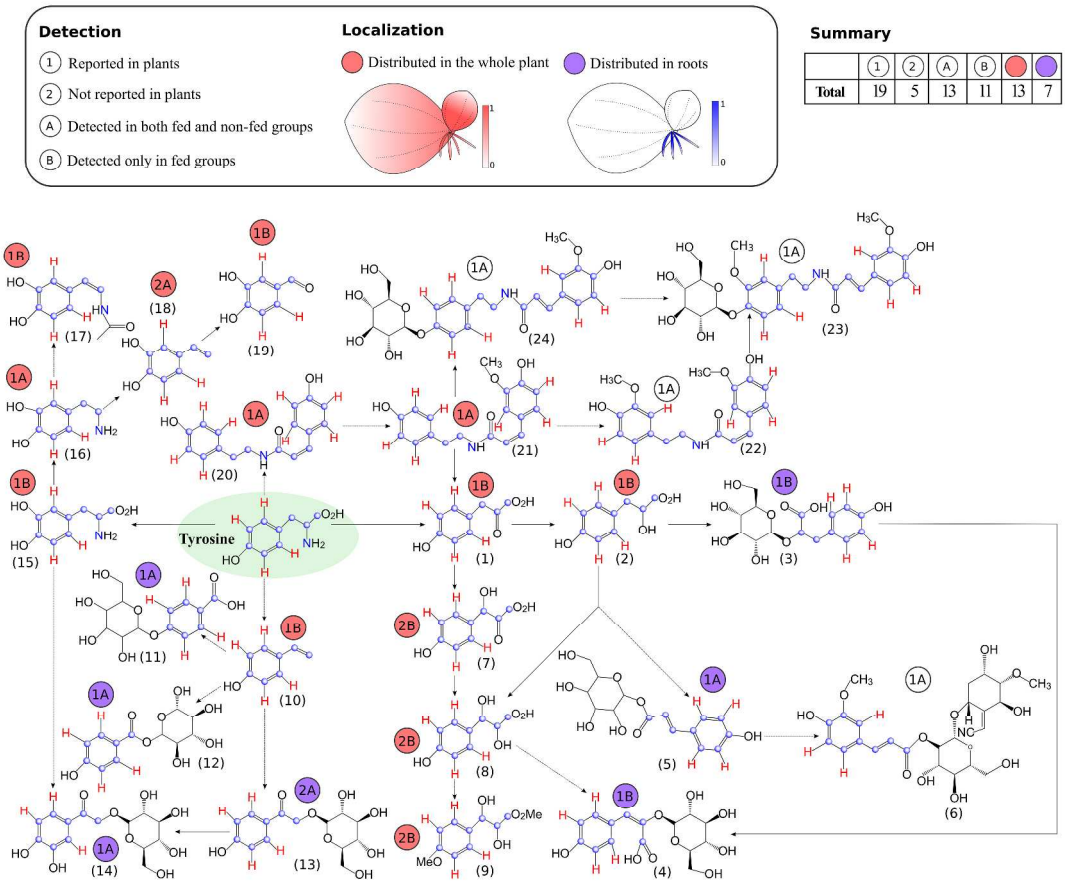

Figure 3. A putative tyrosine-derived metabolic network in Lemna. The pathway was constructed based on possible biochemical reactions using 24 metabolites. Thirteen metabolites are distributed in the whole plant (circled in red), 7 in roots (circled in blue). Nineteen metabolites have been reported in plants (marked with 1) and 5 have never been reported in plants (marked with 2). Thirteen metabolites were detected in both fed and non-fed experiments (marked with A) and 11 were detected in fed experiments.

Stable isotope-labeled internal standard (IS) has been used in quantitative MSI since unlabeled and labeled molecules possess identical ionization efficiency, extractability and MS/MS fragmentation pattern[30,31]. Theoretically, the unlabeled and the corresponding labeled metabolites derived from *in vivo* precursor feeding approach should also possess identical tissue localization pattern in MSI[21]. Fig. 4 (a-b) provides two examples demonstrating the similar localization pattern of unlabeled metabolite and its two labeled forms observed in lemna. In the first example, unlabeled tyrosine and its two labeled forms (Tyr$^{2}H_4$ and Tyr$^{13}C_9{}^{15}N$) were localized homogeneously over the whole lemna plant (Fig. 4a 2-4). The second example is a tyrosine-derived metabolite which has been identified as tyrosine N-carboxyacetyl ($C_{12}H_{13}NO_6$) using DLEMMA-MALDI-Imaging approach (Fig. 4b 6). MALDI images showed that both the unlabeled and the two labeled tyrosine N-carboxyacetyl (m/z+$^{2}H_4$ and m/z+$^{13}C_9{}^{15}N$) were distributed over the whole lemna plant, sharing the same localization pattern (Fig. 4b 2-4).

Notably, in some other cases the unlabeled metabolite and its labeled forms did not show the same tissue localization pattern. Such an example is given in Figure 4c, in which a tyrosine-derived metabolite was identified as lespedezic acid (Fig. 4c 6) in lemna. The unlabeled lespedezic acid was homogenously localized over whole lemna plant (Fig. 4c 2), while the two labeled lespedezic acids were mostly localized in the roots of lemna (Fig. 4c 3-4). The disagreement of the localization pattern between unlabeled and two labeled lespedezic acids was to some extent surprising. Careful investigation of the LC-MS data revealed that the molecular formula of lespedezic acid, $C_{15}H_{18}O_9$, represents at least five isomers. They were retained differently on the reverse phase column, with retention time being 1.31, 2.51, 3.15, 3.59 and 4.16 min (Fig. 4c 5). Out of the 5 isomers, only the isomer eluted at 1.31 min was found to be a tyrosine-derived metabolite as it was the only one that was isotopically labeled. In MSI

experiments, MS images are often reported as ion images in which the *m/z* value of each molecule of interest was used to construct the MS images[1]. Since isomers have identical *m/z* values, the ion image of the 'unlabeled lespedezic acid' shown in Figure 4c-2 in fact represents overlaid ion images of all the five isomers. This also explains why unlabeled and two labeled tyrosine (Fig. 4a 2-4) and tyrosine N-carboxyacetyl (Fig. 4b 2-4) showed the same distribution patterns as no isomers of these two molecules were found in lemna (Fig. 4a 5 and Fig. 4b 5). Differences in distribution patterns between the unlabeled and two labeled lespedezic acid demonstrates a typical case in which structural isomers may be spatially localized in different regions. Hence, in such cases, only ion images of labeled forms (Fig. 4c 3-4) could represent the 'true' localization of metabolites of interest.

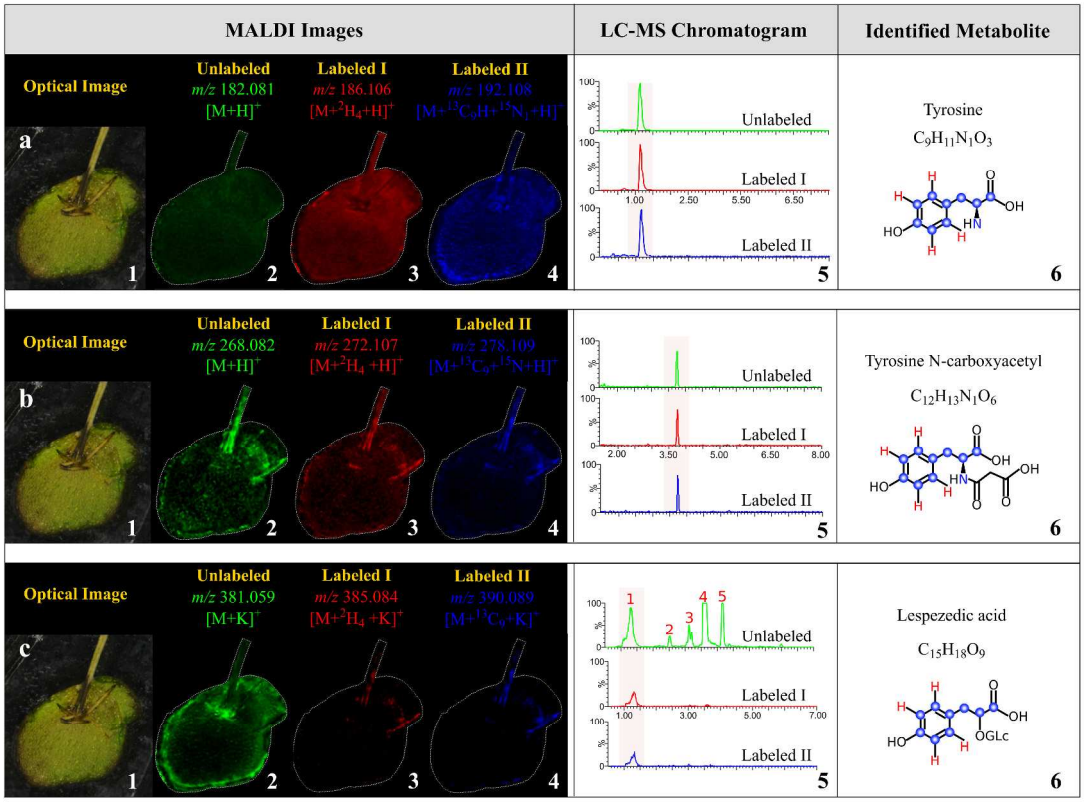

Figure 4. Representative MALDI images of tyrosine-derived metabolites. Tyrosine (a), tyrosine N-carboxyacetyl (b) and lespezedic acid (c) in lemna. (1) Optical image of lemna; MALDI

images showing the distribution of unlabeled (2) and labeled molecules (3-4). The distribution pattern between unlabeled and its two labeled forms are the same for tyrosine and tyrosine N-carboxyacetyl, in which they were localized over the whole lemna tissue. The distribution pattern between unlabeled and two labeled forms were different for lespezedic acid, in which the unlabeled was localized over the whole lemna, while the two labeled forms were mainly distributed in roots. (5) LC-MS chromatograms of the three unlabeled and labeled molecules. (6) The chemical structures of the three molecules with labeling atoms and their positions being highlighted.

Structural isomers exhibit the same molecular formula but different bonding arrangement, which often results in chemically different compounds likely having different biological functions and clinical effects (i.e. pharmacology, toxicology, effects and action on the human body, and legal status)[32,33]. Virtually most metabolites could have one or more structural isomers. In this study, 20-30% of identified metabolites contains at least one structural isomer that have different distribution pattern (Table S1, S2). Consequently, most of the current MSI approaches are likely to generate distorted or obscured MS images due to isomer interferences leading to wrong biological interpretation of the results[34]. The DLEMMA-MALDI-Imaging methodology reported here minimizes isomer interferences by employing two labeled *m/z* values to generate ion images rather than using its unlabeled *m/z*, and therefore reflects the true spatial distribution of metabolites in tissues. Stable isotope labeling is a well-established approach which has been employed to resolve different challenges in metabolomics[35,36]. A successful DLEMMA-MS-imaging experiment largely depends on the labeling patterns of fed precursors since type, number and position of labeled atoms determines the simplicity and efficiency of metabolite

identification. The mode of *in vivo* labeling is another critical factor needs to be optimized per organisms to achieve optimum feeding efficiency. The comprehensiveness of this method is limited as only a particular precursor molecule (e.g., aromatic amino acids) is used for feeding experiments[18], but from the same reason it allows to discover novel metabolites from a specific metabolic pathway.

CONCLUSIONS

In conclusion DLEMMA-MALDI-Imaging offers a number of advantages: (i) it improves metabolite identification; (ii) it increases metabolite coverage via precursor feeding; (iii) it allows construction of a detailed metabolic network map by tracking the specific pathway and most importantly, (iv) it enables precise localization of structural isomers, hence providing the 'true' distribution of molecules of interest. Moreover, this approach can be easily adapted to other MSI modalities such as desorption electrospray ionization (DESI) and secondary ion mass spectrometry (SIMS) imaging, as well as investigation of other living systems.

ACKNOWLEDGEMENTS

We thank the Tom and Sondra Rykoff Family Foundation Research and the Israeli Centers of Research Excellence (i-CORE) program on Plant Adaptation to Changing Environment for supporting the A.A. lab activity. A.A. is the incumbent of the Peter J. Cohn Professorial Chair.

REFERENCES

(1) Dong, Y.; Li, B.; Aharoni, A. *Trends Plant Sci.* **2016**, 21(8), 686-698.
(2) Aichler, M.; Walch, A. *Lab. Investig.* **2015**, *95*, 422-431.
(3) Miura, D.; Fujimura, Y.; Wariishi, H. *J. Proteomics* **2012**, *75*, 5052-5060.
(4) Li, B.; Dunham, S. J.; Dong, Y.; Yoon, S.; Zeng, M.; Sweedler, J. V. *Trends Food Sci. Technol.* **2016**, *47*, 50-63.
(5) Rocha, B.; Ruiz-Romero, C.; Blanco, F. J. *Nat. Rev. Rheumatol.* **2016**, 13, 52-63

(6) Feenstra, A. D.; Hansen, R. L.; Lee, Y. J. *Analyst* **2015**, *140*, 7293-7304.
(7) Dong, Y.; Li, B.; Malitsky, S.; Rogachev, I.; Aharoni, A.; Kaftan, F.; Svatoš, A.; Franceschi, P. *Front. Plant Sci.* **2016**, 7(60), doi: 10.3389/fpls.2016.00060.
(8) Boughton, B. A.; Thinagaran, D.; Sarabia, D.; Bacic, A. *Phytochem. Rev.***2016**. 15, 445-488.
(9) Korte, A. R.; Yandeau-Nelson, M. D.; Nikolau, B. J.; Lee, Y. J. *Anal. Bioanal. Chem.* **2015**, *407*, 2301-2309.
(10) Passarelli, M. K.; Ewing, A. G. *Curr. Opin. Chem. Biol.* **2013**, *17*, 854-859.
(11) Prentice, B. M.; Chumbley, C. W.; Caprioli, R. M. *J. Mass Spectrom.* **2015**, *50*, 703-710.
(12) Lanekoff, I.; Burnum-Johnson, K.; Thomas, M.; Short, J.; Carson, J. P.; Cha, J.; Dey, S. K.; Yang, P. X.; Conaway, M. C. P.; Laskin, J. *Anal. Chem.* **2013**, *85*, 9596-9603.
(13) Perdian, D. C.; Lee, Y. J. *Anal. Chem.* **2010**, *82*, 9393-9400.
(14) Manier, M. L.; Spraggins, J. M.; Reyzer, M. L.; Norris, J. L.; Caprioli, R. M. *J. Mass Spectrom.* **2014**, *49*, 665-673.
(15) Shariatgorji, M.; Nilsson, A.; Goodwin, R. J. A.; Svenningsson, P.; Schintu, N.; Banka, Z.; Kladni, L.; Hasko, T.; Szabo, A.; Andren, P. E. *Anal. Chem.* **2012**, *84*, 7152-7157.
(16) McLean, J. A.; Ridenour, W. B.; Caprioli, R. M. *J Mass Spectrom* **2007**, *42*, 1099-1105.
(17) Trim, P. J.; Henson, C. M.; Avery, J. L.; McEwen, A.; Snel, M. F.; Claude, E.; Marshall, P. S.; West, A.; Princivalle, A. P.; Clench, M. R. *Anal. Chem.* **2008**, *80*, 8628-8634.
(18) Feldberg, L.; Venger, I.; Malitsky, S.; Rogachev, I.; Aharoni, A. *Anal. Chem.* **2009**, *81*, 9257-9266.
(19) Seaman, C.; Flinders, B.; Eijkel, G.; Heeren, R. M.; Bricklebank, N.; Clench, M. R. *Anal. Chem.* **2014**, *86*, 10071-10077.
(20) Louie, K. B.; Bowen, B. P.; McAlhany, S.; Huang, Y.; Price, J. C.; Mao, J.-h.; Hellerstein, M.; Northen, T. R. *Sci Rep.* **2013**, *3*, 1656.
(21) Nakabayashi, R.; Hashimoto, K.; Toyooka, K.; Saito, K. *Anal. Chem.* **2017**, *89*, 2698-2703.
(22) Arts, M., Soons, Z., Ellis, S.R., Pierzchalski, K.A., Balluff, B., Eijkel, G.B., Dubois, L.J., Lieuwes, N.G., Agten, S.M., Hackeng, T.M. and van Loon, L.J., *Angew. Chem. Int. Ed. Engl.* **2017**, 56(25), 7146-7150.
(23) Vunsh, R.; Heinig, U.; Malitsky, S.; Aharoni, A.; Avidov, A.; Lerner, A.; Edelman, M. *Plant Biol.* **2015**, *17*, 115-119.
(24) Itkin, M.; Rogachev, I.; Alkan, N.; Rosenberg, T.; Malitsky, S.; Masini, L.; Meir, S.; Iijima, Y.; Aoki, K.; de Vos, R. *Plant Cell* **2011**, *23*, 4507-4525.
(25) King, R.; Zeevaart, J. *Plant Physiol.* **1974**, *53*, 96-103.
(26) Najla, S.; Vercambre, G.; Génard, M. *Plant Sci.* **2010**, *179*, 316-324.
(27) Smith, C. A.; Want, E. J.; O'Maille, G.; Abagyan, R.; Siuzdak, G. *Anal. Chem.* **2006**, *78*, 779-787.
(28) Oliva, M.; Ovadia, R.; Perl, A.; Bar, E.; Lewinsohn, E.; Galili, G.; Oren-Shamir, M. *Plant Biotechnol. J.* **2015**, *13*, 125-136.
(29) Gustafsson, J. O.; Eddes, J. S.; Meding, S.; Koudelka, T.; Oehler, M. K.; McColl, S. R.; Hoffmann, P. *J. Proteomics* **2012**, *75*, 5093-5105.
(30) Dong, Y.; Guella, G.; Franceschi, P. *Rapid Commun. Mass Spectrom.* **2016**, *30*, 711-718.
(31) Lietz, C. B.; Gemperline, E.; Li, L. *Adv. Drug Deliv. Rev.* **2013**, *65*, 1074-1085.
(32) Reading, E.; Munoz-Muriedas, J.; Roberts, A. D.; Dear, G. J.; Robinson, C. V.; Beaumont, C. *Anal. Chem.* **2016**, *88*, 2273-2280.
(33) Zuba, D.; Adamowicz, P. *Aust. J. Forensic Sci.* **2016**, 1-13.

(34) Li, H.; Smith, B. K.; Márk, L.; Nemes, P.; Nazarian, J.; Vertes, A. *Int. J. Mass Spectrom.* **2015**, *377*, 681-689.
(35) Freund, D. M.; Hegeman, A. D. *Curr. Opin. Biotech.* **2017**, *43*, 41-48.
(36) Chokkathukalam, A.; Kim, D. H.; Barrett, M. P.; Breitling, R.; Creek, D. J. *Bioanalysis* **2014**, *6*, 511-524.

TOC

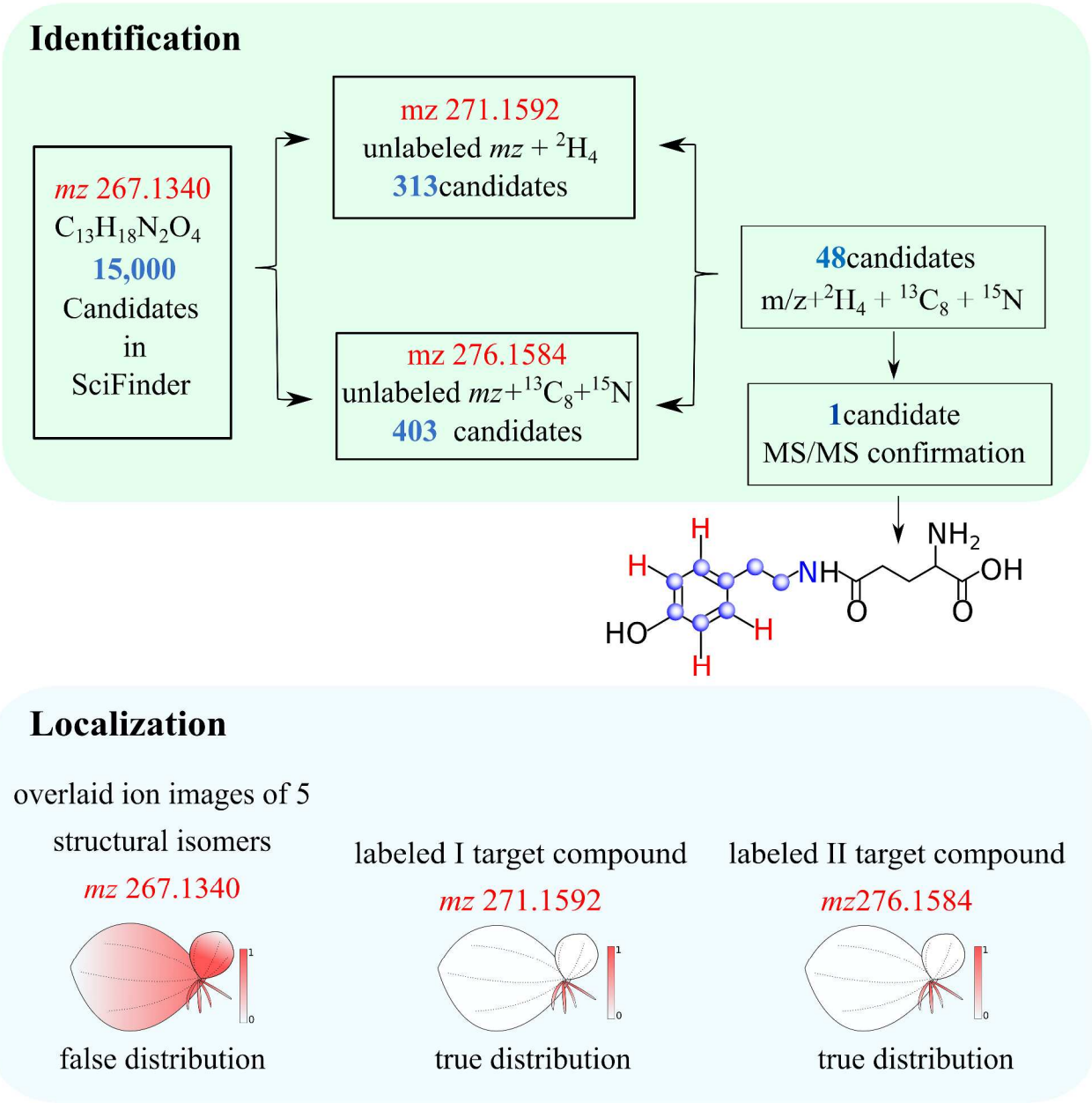
DLEMMA-MS-imaging
Identification
mz 267.1340
$C_{13}H_{18}N_2O_4$
15,000
Candidates
in
SciFinder
mz 271.1592
unlabeled mz + $^2H_4$
313candidates
mz 276.1584
unlabeled mz+$^{13}C_8$+^{15}N
403 candidates
48candidates
m/z+$^2H_4$ + $^{13}C_8$ + ^{15}N
1candidate
MS/MS confirmation
Localization
overlaid ion images of 5
structural isomers
mz 267.1340
false distribution
labeled I target compound
mz 271.1592
true distribution
labeled II target compound
mz276.1584
true distribution